CFD analysis of Jet driven multiphase flow

Azim Memon

Department of Chemical Engineering, Indian Institute of Technology Bombay

Abstract

In industry, Grinding and size reduction at µm scale can be done by the fluidized bed jet mill. The comminution effect is caused by particle-particle collisions in expanding gas streams. Since the common principle of comminution within such a mill is unclear, their construction and output estimation are largely empirical. Using 2.4 mm i.d. nozzles, the effect of free jet velocity set-up geometry on the initial rate of grinding of glass microspheres (soda lime glass) of 5.5 µm size and density 2500 kg/m3 was explored. The numerical simulations helped to better understand the particle–flow interactions in a fluidized bed opposed gas jet mill, which are essential for milling performance.

1. Introduction

In solids processing, grinding is a crucial size reduction process. To crack a particle, the material must be subjected to critical stress. The number of stressing events and their magnitude are determined by the apparatus' configuration. Hammer mills, planetary mills, oscillating mills, and fluidized bed jet mills, etc are widely used in industries because of the stresses caused by mechanical forces. Comminution poses a number of challenges in terms of achieving the best product size and shape delivery, which stem from material characteristics like initial size, material elasticity and plasticity, and process conditions.

The fluidized bed jet mill comprises of three zones. The grinding area at the bottom, where pressurised air is pumped through the nozzles; the transport region in the middle, where the particles are forced upward by the nozzles' gas jets in the grinding region; and the classifying zone at the top where desired particle size are withdrawn.

Just a handful studies have looked into the effects of operation conditions in a fluidized bed opposed jet mill, such as inlet air pressure, and jet nozzle velocity and configuration on particle dynamics operation.

For multiphase modelling of granular flow, i.e. the fluid–solid relationship, the Euler–Euler and Euler–Lagrange approach are frequently used [1, 2]. Just a few computational studies of particle dynamics in fluidized bed jet mills have been done so far [3, 4], while the majority of jet mill simulations are restricted to spiral jet mill systems. [5-9].

As a consequence, the aim of this study is to investigate the particle–fluid interactions behaviour in a fluidized bed opposed jet mill at a fundamental level. To simulate compressible and turbulent gas–solid multiphase flow, authors used the Euler–Euler method, as well as the kinetic theory of granular flow and frictional models. On the particle behaviour, the effects of nozzle inlet air velocity were investigated.

2. Problem Statement

The latest work uses Computational Fluid Dynamics (CFD) technique to evaluate the flow behavior of gas-solid phases while milling process in a fluidized bed jet mill. The current study was carried out with the commercial finite volume based simulator, OpenFOAM (Version 7). Unstructured quadrilateral cells with non-uniform spacing were used to mesh the computational domain. Due to the steep gradients predicted, a very fine mesh was created close to the jet and wall surfaces, and the mesh was gradually coarsened as we moved away from the jet and wall using a particular growth rate parameter. The realisable k–e model modified for turbulent flows is used to concurrently solve the conservation equations of mass and momentum. Air is tangentially fed to the mill at 1, 2 and 3 m/s through the nozzles.

3. Governing Equations

For the gas and solid phases, equations 1 and 2 represent conservation of mass, while equations 3 and 4 represent conservation of momentum.

$$\frac{\partial}{\partial t}\left(\rho_f\,\alpha_f\right)+\nabla.\left(\rho_f\,\alpha_f\,\vec{v_f}\right)=0 \tag{1}$$

$$\frac{\partial}{\partial t}\left(\rho_s\,\alpha_s\right)+\nabla.\left(\rho_s\,\alpha_s\,\vec{v_s}\right)=0 \tag{2}$$

$$\frac{\partial}{\partial t}\left(\alpha_f\,\rho_f\,\vec{v_f}\right)+\nabla.\left(\alpha_f\,\rho_f\,\vec{v_f}\,\vec{v_f}\right)=-\alpha_f\,\nabla p\;+\nabla.\bar{\bar{\tau}}_f+\alpha_f\,\rho_f\,\vec{g}+\left[\beta\left(\vec{v_s}-\vec{v_f}\right)\right] \tag{3}$$

$$\frac{\partial}{\partial t}\left(\alpha_s\, \rho_s\, \vec{v_s}\right) + \nabla.\left(\alpha_s\, \rho_s\, \vec{v_s}\, \vec{v_s}\right) = -\alpha_s\, \nabla p - \nabla p_s + \nabla.\overline{\overline{\tau}}_s + \alpha_s\, \rho_s\, \vec{g} + \left[\beta\left(\vec{v_f} - \vec{v_s}\right)\right] \qquad (4)$$

Where, $\vec{v_f}, \vec{v_s}, \alpha_f, \alpha_s, \rho_f, \rho_s,\ p, p_s, \overline{\overline{\tau}}_f, \overline{\overline{\tau}}_s, \vec{g}$ and β are the gas and solid velocity vectors, the gas and solid volume fractions, the gas and solid densities, the gas and solid pressures, the gas and solid viscous stress tensors, the gravity acceleration vector, and the solid–gas momentum exchange coefficient respectively.

Equation 5 and 6 represent the gas and solid phase stress tensor used in equation 3 and 4 respectively.

$$\tau_g = \mu_g[\nabla U_g + \nabla^T U_g] - \frac{2}{3}\mu_g(\nabla.U_g)I \qquad (5)$$

$$\tau_s = \mu_s[\nabla U_s + \nabla^T U_s] - \left(\lambda_s - \frac{2}{3}\mu_s\right)(\nabla.U_g)I \qquad (6)$$

GidaspowWenYu model:

Wen-Yu model (1966)
$$K_{gs} = \frac{3}{4}C_D\frac{\alpha_g\alpha_s\rho_g}{d_p\alpha_g^{2.65}}\left|\vec{v_g} - \vec{v_s}\right|$$

Gidaspow model (1994)
$$K_{gs} = 150C_D\frac{\alpha_s\mu_g}{\alpha_g d_p^2}\left(1 - \alpha_g\right)$$
$$+1.75\frac{\alpha_g\rho_g}{d_p}\left|\vec{v_g} - \vec{v_s}\right| \qquad ;\ \text{for} \quad \alpha_g \leq 0.8$$

Now, GidaspowWenYu model; when $\alpha_g \geq 0.8$
$$C_D = \frac{24}{\alpha_g Re_s}\left(1 + (0.15\alpha_g Re_s)^{0.687}\right)$$
$$Re_s = \rho_g\frac{d_p}{\mu_g}\left|\vec{v_g} - \vec{v_s}\right|$$

4. Simulation Procedure

The simulation is performed in the OpenFOAM simulator (Version 7) with the initial and boundary conditions listed in the boundary condition section. The post processing is done in ParaView, version 5.9.0.

The PIMPLE algorithm was used for pressure-velocity coupling which is blend of the SIMPLE (Semi-Implicit Method for Pressure-Linked Equations) and PISO (Pressure-Implicit with Split-Operator) algorithms. For modelling turbulence in multiphase flows, the traditional k-dispersed

turbulence model was chosen (dual phase for jet mill). For convergence, the residual for each governing equation was held below 10^{-5} fort each time step.

Transport equations were numerically discretized using second-order discretization schemes (divergence, Laplacian, and gradient terms). For all unsteady terminology, the implicit Euler scheme with first-order bounds was used (i.e., temporal discretization). The simulations in this study used a time step of about 10^{-5} seconds. Pressure, velocities, volume fractions and k-ε variables had their convergence parameters set to 10^{-8}, 10^{-5}, 10^{-9} and 10^{-5} respectively.

The Courant number was held less than 0.5 for a time-accurate solution, even though an implicit scheme was used [10].

4.1 Geometry and Mesh

Figure 1 shows a detailed representation of the fluidized bed opposed gas jet mill as well as all of the geometric parameters. The geometry and computational mesh is built in commercial software ANSYS Fluent (Version 21.1). Unstructured quadrilateral cells with non-uniform spacing were used to mesh the computational domain. Due to the steep gradients predicted, a very fine mesh was created close to the jet and wall surfaces, and the mesh was gradually coarsened as we moved away from the jet and wall using a particular growth rate parameter as shown in **Figure 2**.
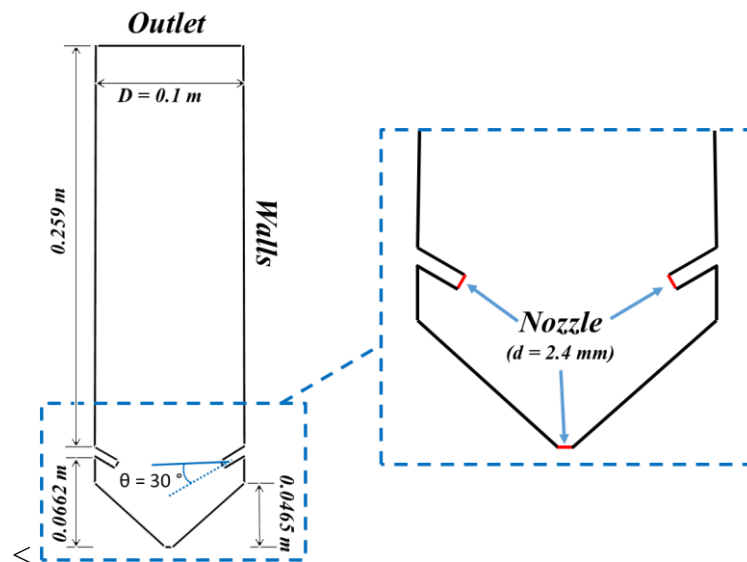

Figure 1. Schematic representation of the computational domain.

Grid consisting of 10 control volumes on the jet surface, 8788 control volumes in the entire computational domain with a smallest grid size of 2.47×10^{-3} m and average surface arear

3.045×10^{-2} m² were thought to be adequate for capturing the prevailing steep velocity gradients in the boundary layers and for the present numerical results to be grid-free.
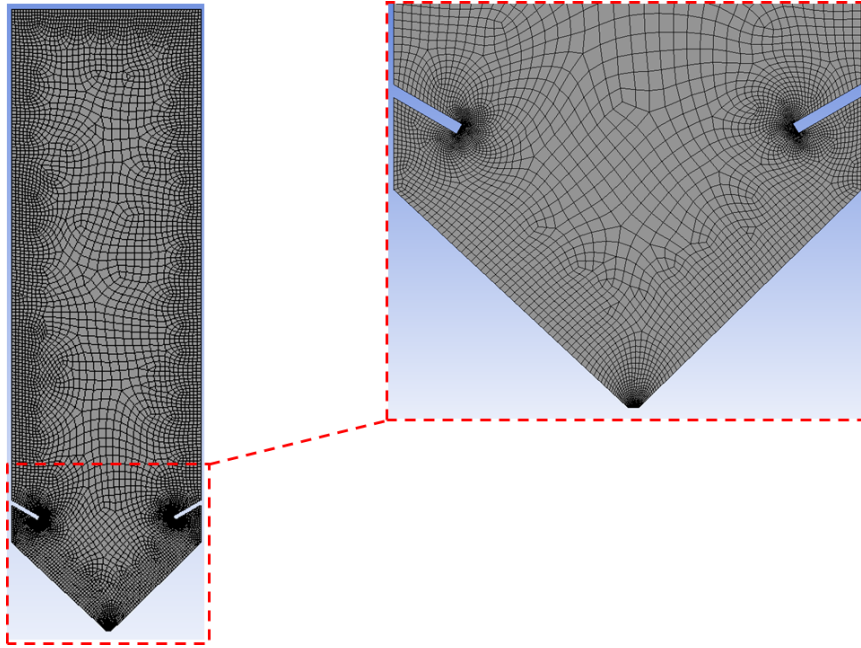

Figure 2. Meshing of the computational domain.

4.2 Initial and Boundary Conditions

For the fluidized bed geometry and operating conditions, simulations were based on experimental works in the literature. [11, 12, 13].

Figure 3. Initial particle bed condition in Euler-Euler simulation (h = 0.0683 m).

A velocity-inlet boundary condition was used to implement the gas flow equally from all three nozzles. The top of the bed was designated as a pressure outlet, and the boundary walls were given no-slip boundary conditions for air and partial-slip boundary condition for particles. Only the air flow was able to escape through the top of the equipment. For the solid hold up, the initial particle bed height is taken to be 0.0683 m as shown in figure 3. Air is tangentially fed to the mill at 1, 2 and 3 m/s through three the nozzles. One nozzle is at bottom of the particle bed, whereas other two nozzles are placed at height of 0.662 m from the bottom (figure 1) and they are apart by 65.4 mm and are inclined at an angle of 30°.

4.3 Solver

OpenFOAM, which uses twoPhaseEulerFoam solver, employs the Euler-Euler approach for simulation. twoPhaseEulerFoam is a solver for a non-reacting compressible fluid phase system of two non-reacting fluid phases. In this scheme, one step is always dispersed. As a result, it's an excellent candidate for simulating bubble columns in gas/liquid systems, as well as fluidized beds and spouted beds in gas/solid systems.

In the case of gas-liquid systems, all phases can be modelled using laminar and turbulence models (RAS and LES). Only the fluid phase of gas-solid or liquid-solid systems can be extended with these models. The strong phase momentum equation includes a model for the stress tensor.

5. Results and Discussions

As a function of nozzle inlet velocity, the time-averaged particle volume fraction distribution across the fluidized bed opposed jet mill is shown in **Figure 4 (1 m/s, 2 m/s, 3 m/s).** It is clearly seen from the contours that the fluidized bed height increases with increasing velocity as well as time.

Figure 5 plots the time-averaged particle volume fraction over the axial line at the equipment's centre, which includes the grinding and transporting regions. As shown in **Figure 4**, as a function of axial position, very low solid volume fractions were observed in the fluidized bed, with maximum values at the grinding region and decreasing towards the transport region **(Figure 5)**.

Figure 6 shows that regardless of the nozzle inlet velocity values, particle concentrations are low in the centre and rise towards the fluidized bed wall, resulting in a core-annulus flow.
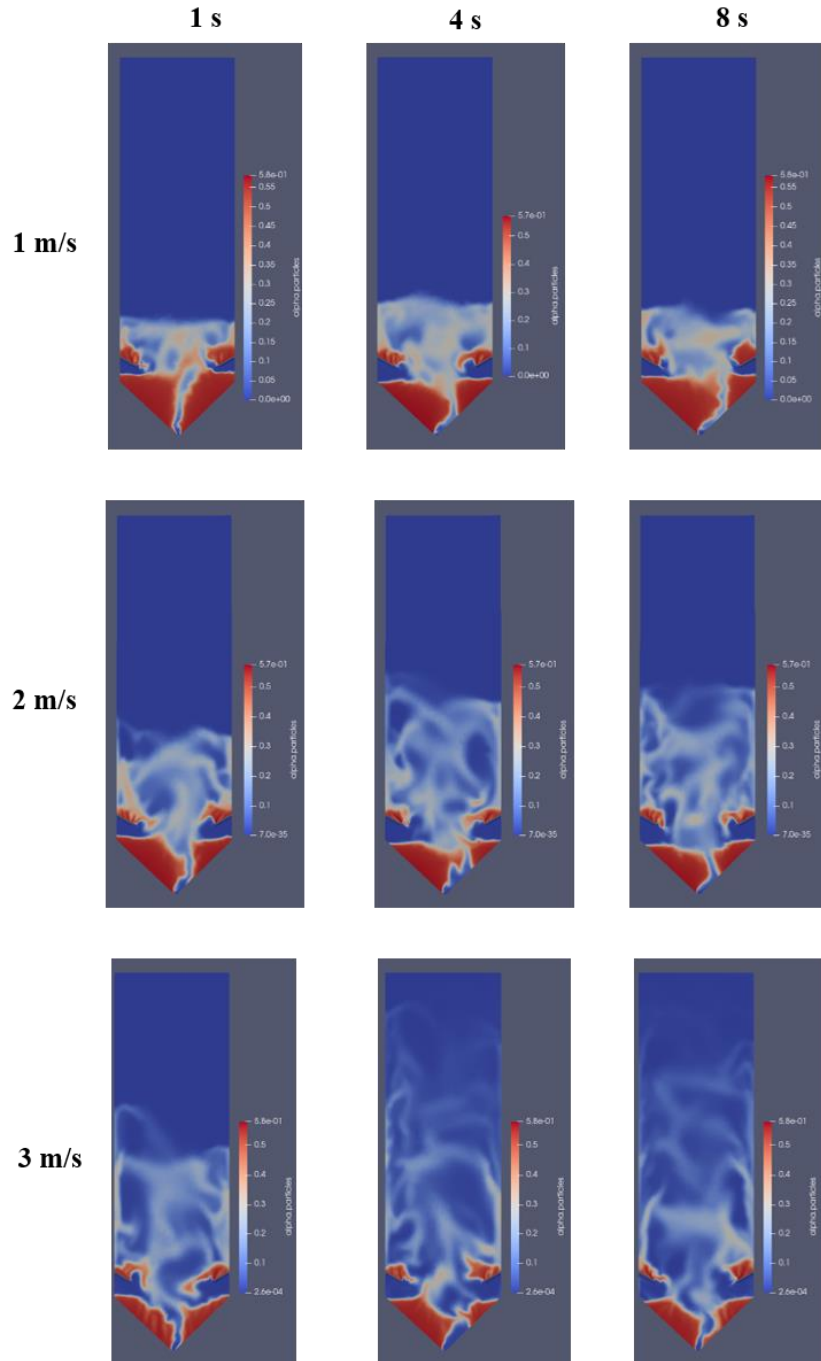
Figure 4. Time-averaged particle volume fraction distribution as a function of nozzle inlet velocity (1 m/s, 2 m/s, 3 m/s).

This section systematically examines the time-averaged velocity and time-averaged volume fraction distributions of both phases to throw new light on the complex particle–fluid behaviour within a fluidized bed gas opposed jet mill.
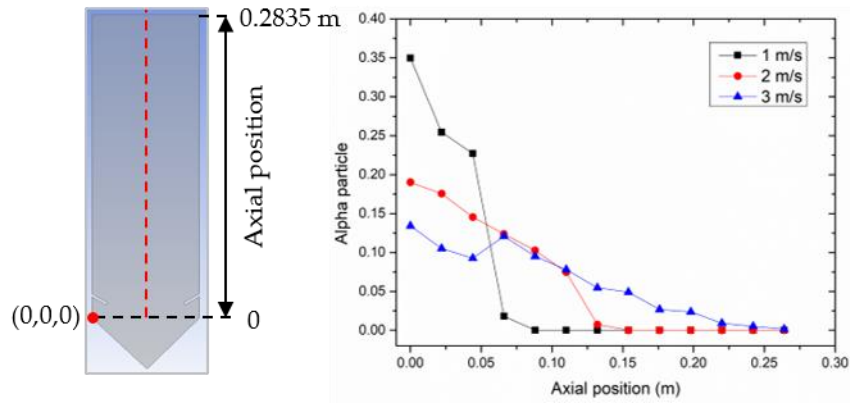
Figure 5. Axial distribution of the time-averaged solid volume fraction at a fixed axial position of 0.05 m from the equipment origin.
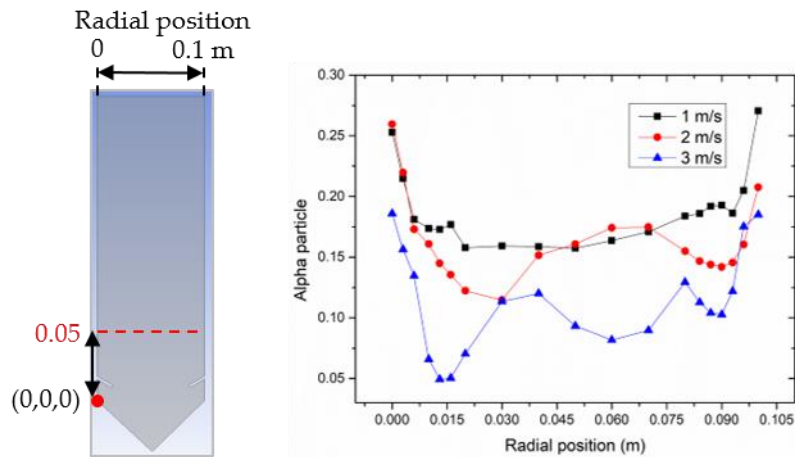

Figure 6. Radial distribution of the time-averaged solid volume fraction at a fixed axial position of 0.05 m from the equipment origin.

Figures 7 show the velocity profile for the air and particulate phases at different inlet speeds.

Figure 8 shows the time-averaged particle velocity along the axial line through the middle of the equipment, from the origin to the transport field, to further investigate this observation. The maximum value of particle is for the case of jet velocity 3 m/s.

Positive values were found in the fluidized bed's middle, while negative values were found along the wall, indicating that particles are flowing back to the grinding region along the wall, as stated previously (figure 9).
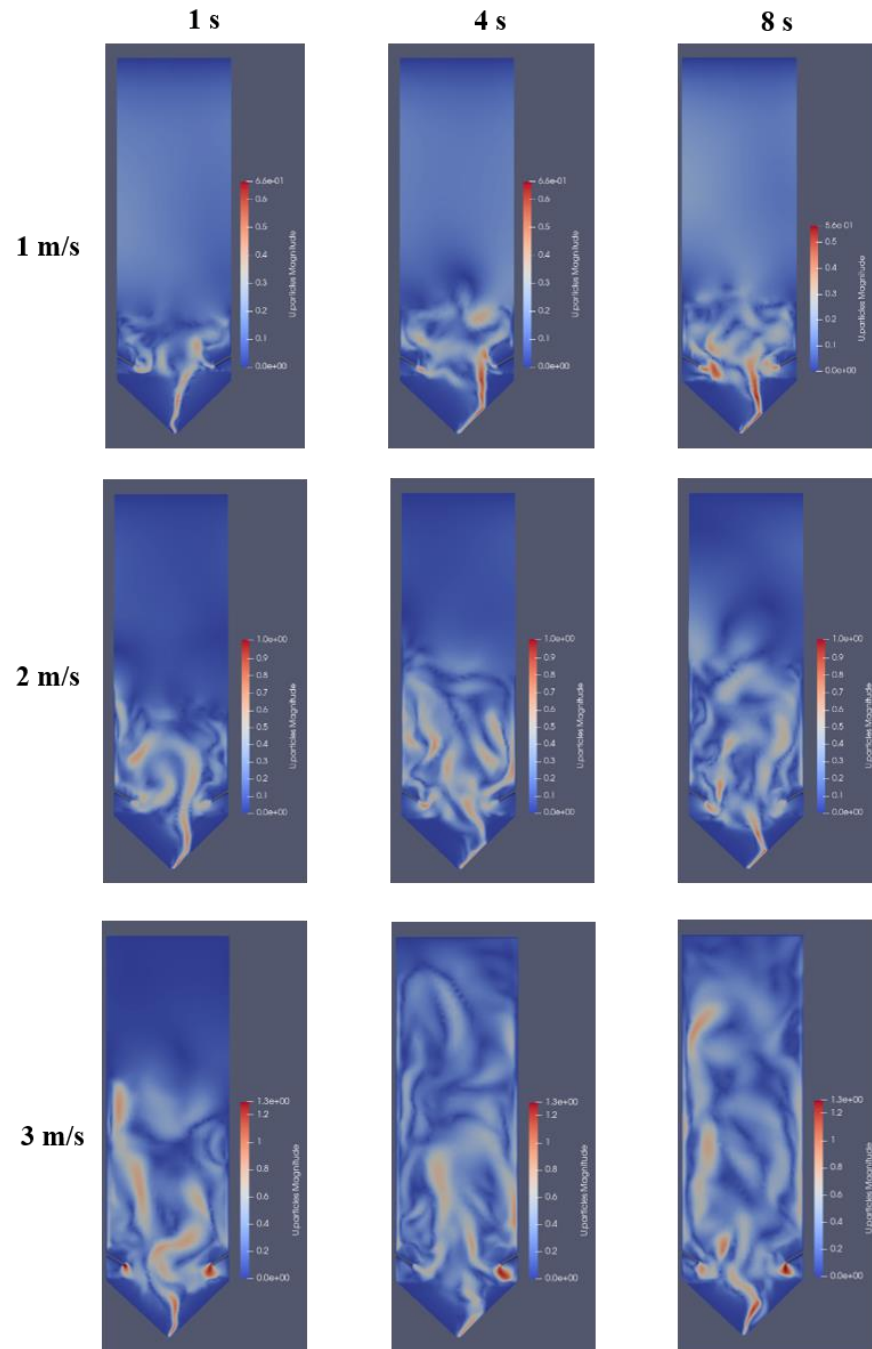
Figure 7. Time-averaged particle velocity distribution as a function of nozzle inlet velocity (1 m/s, 2 m/s, 3 m/s).
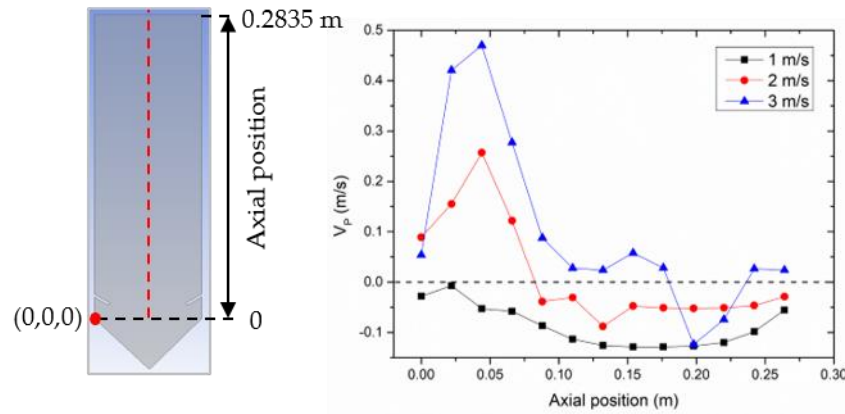
Figure 8. Axial distribution of the time-averaged particle velocity at a fixed axial position of 0.05 m from the origin.
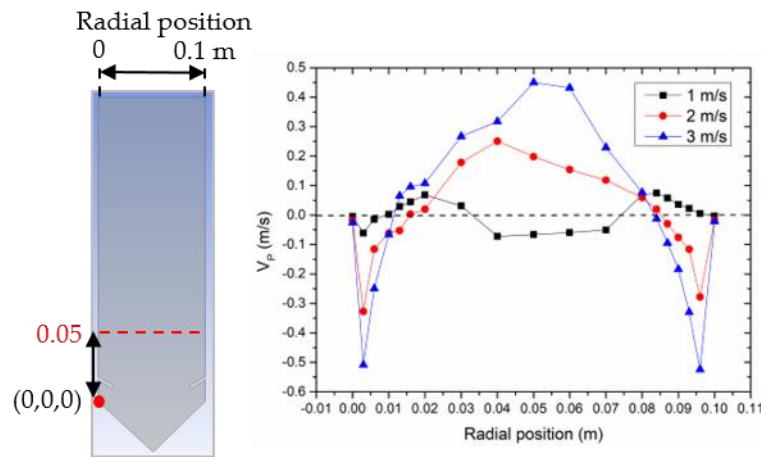

Figure 9. Radial distribution of the time-averaged particle velocity at a fixed axial position of 0.05 m from the origin.

Conclusion

The Euler-Euler method was used to examine gas-solid multiphase flow within an opposed gas jet fluidized bed, as well as the kinetic theory of granular flow and frictional models. The solids movement and concentration inside the apparatus were modelled using this method under various operating conditions.

The particle and fluid flows exhibited asymmetric behaviour, suggesting spatial and temporal periodic behaviour within the apparatus. These oscillations can have an impact on particle residence time and stressing conditions in the grinding zone, as well as particle transport to the top.

Not only particle-particle interaction is responsible for reduction in size but also interaction between particle-particle was observed at walls of equipment suggesting that particle breakage and comminution efficiency are encouraged not only by the air jets but also by the equipment walls.

References

1. Jiang, Z.; Hagemeier, T.; Bück, A.; Tsotsas, E. Color-PTV measurement and CFD-DEM simulation of the dynamics of poly-disperse particle systems in a pseudo-2D fluidized bed. Chem. Eng. Sci. 2018, 6, 115–132.

2. Benedito, W.M.; Duarte, C.R.; Barrozo, M.A.S.; Santos, D.A. An investigation of CFD simulations capability in treating non-sphericalparticle dynamics in a rotary drum. Powder Technol. 2018, 332, 171–177.

3. Rajeswari, M.S.R.; Azizli, K.A.M.; Hashim, S.F.S.; Abdullah, M.K.; Mujeebu, M.A.; Abdullah, M.Z. CFD simulation and experimental analysis of flow dynamics and grinding performance of opposed fluidized bed air jet mill. Int. J. Miner. Process. 2011, 98, 94–105.

4. Lee, H.W.; Song, S.; Kim, H.T. Improvement of pulverization e_ciency for micro-sized particles grinding by uncooled high-temperature air jet mill using a computational simulation. Chem. Eng. Sci. 2019, 207, 1140–1147.

5. Teng, S.;Wang, P.; Zhu, L.; Young, M.-W.; Gogos, C.G. Experimental and numerical analysis of a lab-scale fluid energy mill. Powder Technol. 2009, 195, 31–39.

6. Teng, S.;Wang, P.; Zhang, Q.; Gogos, C. Analysis of Fluid Energy Mill by gas-solid two-phase flow simulation. Powder Technol. 2011, 208, 684–693.

7. Brosh, T.; Kalman, H.; Levy, A.; Peyron, I. Francois R. DEM-CFD simulation of particle comminution in jet-mill. Powder Technol. 2014, 257, 104–112.

8. Rodnianski, V.; Levy, A.; Kalman, H. A new method for simulation of comminution process in jet mills. Powder Technol. 2019, 343, 867–879.

9. Bnà, S.; Ponzini, R.; Cestari, M.; Cavazzoni, C.; Cottini, C.; Benassi, A. Investigation of particle dynamics and classification mechanism in a spiral jet mill through computational fluid dynamics and discrete element methods. Powder Technol. 2020, 364, 746–773.

10. Dyrney Araújo dos Santos, Shivam Baluni and Andreas Bück, Eulerian multiphase simulation of the particle dynamics in a fluidized bed opposed gas jet mill. Processes. 2020, 8. 1621.

11. Köninger, B.; Hensler, T.; Romeis, S.; Peukert,W.;Wirth, K.-E. Dynamics of fine grinding in a fluidized bed opposed jet mill. Powder Technol. 2018, 327, 346–357.

12. Köninger, B.; Spoetter, C.; Romeis, S.;Weber, A.P.;Wirth, K.-E. Classifier performance during dynamic fine grinding in fluidized bed opposed jet mills. Adv. Powder Technol. 2019, 30, 1678–1686.

13. Köninger, B.; Kögl, T.; Hensler, T.; Arlt,W.;Wirth, K.-E. Solid distribution in fluidized and fixed beds with horizontal high speed gas jets. Powder Technol. 2018, 336, 57–69.